Contribution of the ventral pouch in the production of mouse ultrasonic vocalizations

S. Abhirami,[1,2] Swapna Agarwalla,[1,3] Anandaroop Bhattacharya,[2] and Sharba Bandyopadhyay[1,3,*]

[1]*Information Processing Laboratory, Indian Institute of Technology Kharagpur, Kharagpur 721302, India*

[2]*Department of Mechanical Engineering, Indian Institute of Technology Kharagpur, Kharagpur 721302, India*

[3]*Department of E&ECE, Indian Institute of Technology Kharagpur, Kharagpur 721302, India*

(Received 6 June 2022; revised 20 October 2022; accepted 21 December 2022; published 21 February 2023)

Mouse ultrasonic vocalizations (USVs) are of communicative significance and can serve as one of the major tools for behavioral phenotyping in mouse models of neurological disorders with social communication deficits. Understanding and identifying the mechanisms and role of laryngeal structures in generating USVs is crucial to understanding neural control of its production, which is likely dysfunctional in communication disorders. Although mouse USV production is accepted to be a whistle-based phenomenon, the class of whistle is debatable. Contradictory accounts exist on the role of a specific rodent intralaryngeal structure—the ventral pouch (VP), an air-sac-like cavity, and its cartilaginous edge. Also, inconsistencies in the spectral content of fictive USVs and real USVs in models without the VP points us to re-examine the role of the VP. We use an idealized structure, based on previous studies, to simulate a two-dimensional model of the mouse vocalization apparatus with the VP and without the VP. Our simulations were performed using COMSOL Multiphysics to examine characteristics of vocalizations beyond the peak frequency (f_p), like pitch jumps, harmonics, and frequency modulations, important in context-specific USVs. We successfully reproduced some of the crucial aspects of mouse USVs mentioned above, as observed through the spectrograms of simulated fictive USVs. Conclusions about the lack of a role of the mouse VP were previously made in studies primarily examining f_p. We investigated the impact of the intralaryngeal cavity and the alar edge on the simulated USV features beyond f_p. For the same combinations of parameters, removing the ventral pouch resulted in an alteration of the call characteristics, dramatically removing the variety of calls observed otherwise. Our results thus provide evidence supporting the hole-edge mechanism and the possible role of the VP in mouse USV production.

DOI: 10.1103/PhysRevE.107.024412

I. INTRODUCTION

Sound is one of the primary media of communication for humans as well as for animals. Mice emit vocalizations both in the human audible and inaudible range (beyond 20 kHz) [1,2]. However, the ones emitted in the ultrasonic range are vital as they hold the potential of eliciting change in behavior at the receiver end. For example, pup ultrasonic vocalizations (USVs), also known as isolation calls, induce a search and retrieval behavior in the mother [3] and allow for individual recognition [4]. In adult males, USVs are in synchrony with specific behavior such as nosing and mounting females [5,6]. Given the above aspects, mouse USVs are of communicative significance [7] and can be used as an index of maturation, responsiveness, emotional states, and drug treatment [2,8]. An understanding of the relationship between USV production and the descending motor control signals driving them is crucial since any alteration in USVs can serve as a translational tool for linking genetic mutations to speech and communication deficits [8–10]. However, there are diverse opinions about the mechanism that regulates the production of these USVs.

The acoustic sound generation in pipes or wind instruments pertains to different geometries and frequency range compared to mouse USVs [11]. If we consider the flute, which is one of the high frequency wind instruments, the cutoff frequencies are in the range of 3 kHz for classical, Baroque, or modern flutes [12]. Therefore, the studies on wind instruments, especially frequency spectra, cannot be readily extended to mouse USVs. Moreover, such ultrasonic phenomena have been reported previously only in industrial supersonic and subsonic flows [13] and thereby the mechanism of USV production in mice is unique to mammals.

That mice USVs are governed by a whistle-based mechanism was demonstrated by Robert in 1975 [14] with the help of heliox experiments. Replacing oxygen with a light density gas, helium, changed the fundamental frequency (f_0) of USVs as a velocity function, which did not hold for audible cries in mice. The experiment proved that mice USVs cannot be produced by vibrating structures, thereby leading to the postulation of the presence of some whistle-based mechanism. Whistles are generated when some disturbance creates instability in the smooth laminar flow of a fluid and causes the stream to form periodically spaced vortices that give rise to oscillations in the surrounding fluid [15]. Though the disturbance may not be sustained, the oscillations can be. However, the class of whistle to which USVs belong still remains controversial.

Chanaud's work in 1970 [15] gives an introduction to the various types of whistles, among which hole tone [14], hole

*Corresponding author: sharba@ece.iitkgp.ac.in

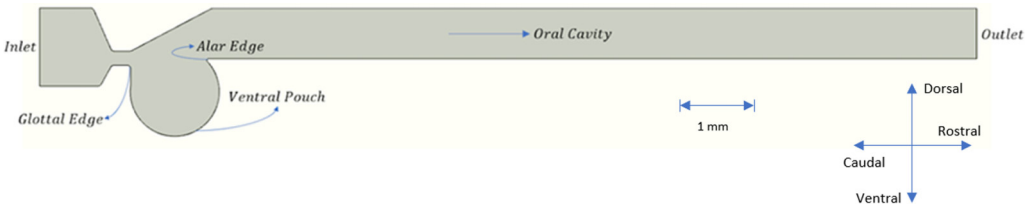

FIG. 1. Geometry of the laryngeal airflow. The alar edge, glottal edge, ventral pouch, oral cavity, along with inlet and outlet are marked.

edge [16], and jet impingement mechanisms [17,18] have been considered by others in the context of USV generation. Robert's work in 1975 [14] supported the hole tone model requiring two orifices in the laryngeal cavity. Later, anatomical observations proved that the hole tone setup is unlikely since a second orifice is absent. In 2016, Mahrt [17] provided theoretical and experimental evidence for the jet impingement mechanism where they claimed that the jet was getting impinged on the interlaryngeal wall. However, Mahrt's proposed mechanism became questionable when Riede's 2017 [16] work with three-dimensional (3D) reconstructed CT scans of the laryngeal airways of different mice families found no physical existence of planar surfaces for the jet to impinge on and on taking into consideration the relevance of two more structures, namely alar edge and ventral pouch, which have been reported previously in multiple studies [19,20], found alteration in USV production on damaging the ventral pouch. The scans revealed that the typical mouse laryngeal pathway from the trachea to the oral cavity consists of a constriction in the glottis, followed by a pouchlike cavity termed a ventral pouch (VP) ending in an edgelike structure known as alar cartilage. The presence of the above anatomical structures led to the hypothesis that it might act like a jet-edge system with a resonator, wherein the source of disturbance is the edge placed in the path of jet flow. The alar edge was surgically damaged to observe the effects on the output sound. Interestingly, although a complete loss of USV production was rarely observed, there was a significant change in vocalizations, providing evidence in support of the hole-edge mechanism [16]. Later, in 2020, Riede [21] further confirmed the importance of the distance between the glottis and alar edge as well as the volume of VP in regulating the fundamental frequency.

A more recent work, however, made a comparative study of the three intralaryngeal mechanisms, namely, the wall impingement, alar edge impingement, and shallow cavity tone [18]. This study provides physiological and 3D simulations in support of the jet impingement mechanism, concluding that the VP and the alar edge are irrelevant for USV production as they found no difference in the peak frequency f_p) of output sound with and without blocking VP [18]. Although f_p is one of the essential features, replicating merely f_p by blocking VP may not be sufficient to conclude that vocalizations do not undergo any change and that the VP has no role. The sudden change in frequency, harmonics, and presence of nonlinear components are a few of the characteristics of the subtypes of the mouse USVs [1,2,10,22,23] which, although distinctly different from each other spectrographically, can have the same f_p. This was not considered in the above study. Moreover, blocking the VP with an aluminum ball might serve the purpose of filling the VP but it leads to the creation of a new curvaturelike surface in its place. The presence of such nonlinear structures in lieu of the VP may fail to capture the importance of the VP in USV production and thereby leads to uncertainty about the underlying mechanism as claimed in their work. Therefore, there is a need for reinvestigating the role of the VP and alar edge without creating any new surfaces and validate the mechanism involved in generating USVs.

In our study, we simulated a 2D model in COMSOL Multiphysics replicating the anatomical structures as reported using contrast-enhanced microCT scans by Riede in 2017 [16]. The geometry used for simulation is similar to Fig. 8(c) in Riede *et al.* 2017 [16] which is a figure used to illustrate the mechanism of the edge-tone model. The dimensions of the model under study are based on Fig. 5(c) in Riede 2017 [16] which represents the midsagittal dimensions of the airways of the grasshopper mouse and has a diameter of 1.2 mm. We use an idealized version of the geometry, as it can serve as the basis for insight into how impactful the geometrical intricacies are as we move from the ideal to realistic models. For CT scan based geometries also, there are similar problems as no two mice would be the same and is dependent on the state of the animal in which the scan is done. We wanted to use specific components that are well understood in physics like a Helmhotz oscillator (which is the ventral pouch) in conjunction with other components. Hence our question is specifically to do with the geometrical feature (or anatomical structure), the ventral pouch, whose contribution to mouse USVs has been ruled out.

Our model successfully reproduced some of the spectrograms as observed in the mouse USVs. To further understand the role of the VP, instead of filling it with a metallic ball as reported in one of the recent works, we opted for removing the VP. Spectrographic analysis of the output of the simulations with and without VP resulted in alteration of the USV characteristics. Therefore, our simulations validate the role of VP and alar edge in mouse USV production through the hole-edge mechanism as suggested by Riede in his works [16,21].

II. 2D MODEL OF THE MOUSE LARYNX AIRWAY

In this study, a 2D model of a mouse laryngeal airway is simulated by recreating the CT scans close to the dimensions reported in Reide 2017 [16]. COMSOL Multiphysics version 5.5 is used for computational fluid dynamics simulations of the airflow through a laryngeal airway model and the schematic of the same is shown in Fig. 1. The airflow through the model is defined as laminar and compressible. A nonpenetration nonslip condition is applied at the laryngeal wall, the meshing is automatic, and a zero gauge pressure boundary condition is applied at the outlet. The mesh in the geometry

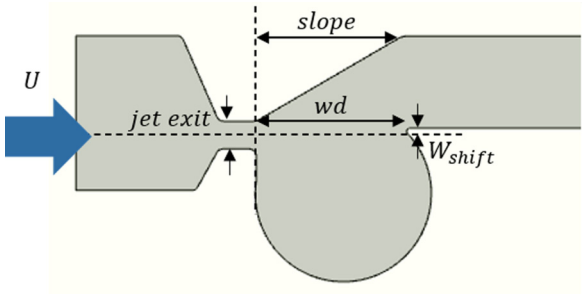

FIG. 2. Parameters varied for simulation. The vertical position of the alar edge W_{shift}, slope (S_p), wedge distance (w_d) jet exit diameter (D_j), and inlet velocity (U_{in}) are marked.

had to be locally adjusted to capture the flow patterns. While a systematic grid independent study could not be done due to the complex geometry involving multiple constrictions and expansions, the mesh parameters were locally adjusted and refined in order to capture the local velocity and pressure contours accurately. The local refinements were done to a point where the flow patterns and values were no longer altered any further. For the temporal resolution, the time step was chosen corresponding to 250 kHz which was the highest frequency studied. The equations solved by the laminar flow interface are the Navier-Stokes equations for conservation of momentum, and the continuity equation for conservation of mass. The equations governing the simulations are given below:

$$\frac{\partial \rho}{\partial t} + \nabla \cdot (\rho u) = 0, \tag{1}$$

$$\left\{\rho\left(\frac{\partial u}{\partial t} + u \cdot \nabla u\right)\right\}_1 = \left\{\nabla \cdot \left[\mu\left(\nabla u + (\nabla u)^T - \frac{2}{3}\mu(\nabla \cdot u)I\right)\right]\right\}_2 + \{-\nabla \rho\}_3 + \{F\}_4, \tag{2}$$

where ρ is the fluid density, u is the fluid velocity vector, μ is the fluid dynamic viscosity, and $\{\}_1$ corresponds to the inertial forces, $\{\}_2$ to the viscous forces, $\{\}_3$ to the pressure forces, and $\{\}_4$ to the external forces applied to the fluid.

A. Simulation results and analysis

The parameters varied in the simulations are the vertical position of the alar edge W_{shift}, its distance from the glottal edge w_d, and the slope of the upper portion to the right of the jet exit S_p and D_j as marked in Fig 2. We use the center point of the parameter space based on the geometry in Reide *et al.* 2017. Next we vary them to the range 10–20%. Some of these are corroborated based on data of Håkansson 2022 [18] and similar ranges of percentage changes are studied in terms of tracheal diameter in humans [24]. The only user-defined nongeometric parameter is the inlet velocity of air U_{in} and is

TABLE I. Parameters of the 2D model.

Parameter	Range
Steady state inlet velocity U_0	[6.4, 9.6 ms^{-1}],
w_d	[0.8, 1.1 mm]
W_{shift}	[−0.045, +0.045 mm], W_{shift}=0 corresponds to the line vertically bisecting the jet exit
S_p	[0.75, 1.1 mm]
D_j	[0.17, 0.21 mm]

defined as

$$U_{\text{in}}(t) = 2U_0\left(\frac{1}{1+e^{-\lambda t}} - 0.5\right), \tag{3}$$

where U_0 is the steady state asymptotic value of the (actual, physical) inlet velocity with $\lambda = 1000\,\text{s}^{-1}$ and U_0 varies between 6.4 and 9.6 ms^{-1}. The inlet velocity starts at 0 at $t = 0$ and then increases smoothly to avoid unphysical transients to reach the steady state value of U_0 in the simulation. The above rise is not any phenomenon in the mouse vocalization production, but only to avoid unwanted transients in the simulations. The ranges of values of the different parameters and the reasoning behind the selection of these ranges have been tabulated in Table I.

The range of air pressure (p) inside the vocal tract of mice ranges within [0, 2 kPa] [18]. The model was run for different inlet velocity inputs to identify the extreme value, i.e., corresponding to $p \sim 2$ kPa. Since the overall cavity has several sections with different cross sectional areas, as well as sudden expansions and contractions along with a ventral pouch, the simple relation for frictional pressure drop for flow through a pipe/channel given by

$$\Delta p = p_{\text{in}} - p_{\text{out}} = f\left(\frac{L}{D}\right)\rho\left(\frac{U_{\text{in}}^2}{2}\right) \tag{4}$$

may not be valid and lead to underpredictions. Therefore, we used the numerically obtained pressure drop data values for different inlet velocities to calculate the loss coefficient using $\Delta p = K\rho(\frac{U_{\text{in}}^2}{2})$. The loss coefficient for our geometry was found to be 43.66. It may be noted that the outlet pressure boundary condition in our model was set to atmospheric pressure or gauge pressure of zero. As a result, the inlet gauge pressure p_{in} is numerically equal to Δp.

After setting the parameters, a time-dependent study is run with a step size of $\Delta t = 1/S_f$, where S_f is the sampling frequency. We record the pressure values at the output point marked red as shown in Fig. 3.

To understand the variation in the output sound characteristics with different parameters such as U_0, w_d, and others,

FIG. 3. Output point (red) where pressure values are recorded.

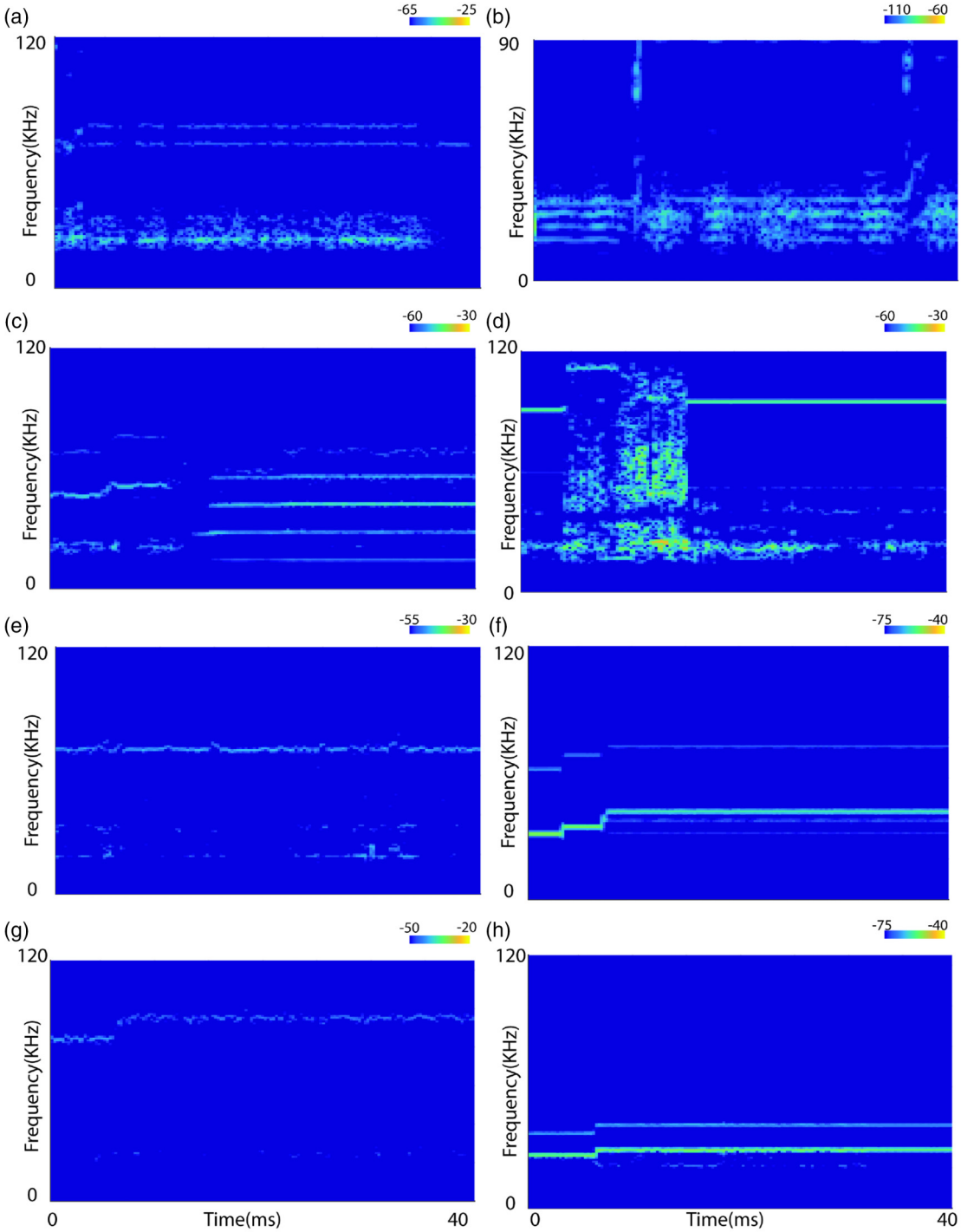

FIG. 4. Example of spectrograms generated. (a) Three component nonharmonic relation. (b) Low frequency harmonics. (c) Harmonic change in fundamental, number of components, modulations. (d) Single frequency contour interrupted by noise in between. (e) Single frequency contour (almost flat). (f) Harmonic with two components. (g) Single frequency contour with sudden change in fundamental frequency. (h) Nonharmonic with two components.

pressure versus time data sets are being recorded. The pressure signals are passed through a bandpass Butterworth filter of order 9 with the minimum and maximum limit set to 20 and 120 kHz respectively. Spectrograms of the pressure signals are then computed in MATLAB 2015a using a Hamming window of length 256 and an overlap of 75% by calling an inbuilt function "spectrogram." The inbuilt function spectrogram in MATLAB computes the short-time Fourier transform (STFT) to analyze how the frequency content of a signal changes over time. The STFT of a signal is computed by sliding a hamming window $g(n)$ of length M over the signal and calculating the discrete Fourier transform (DFT) of each segment of windowed data. The window hops over the original signal at intervals of R samples, equivalent to $L = M - R$ samples of

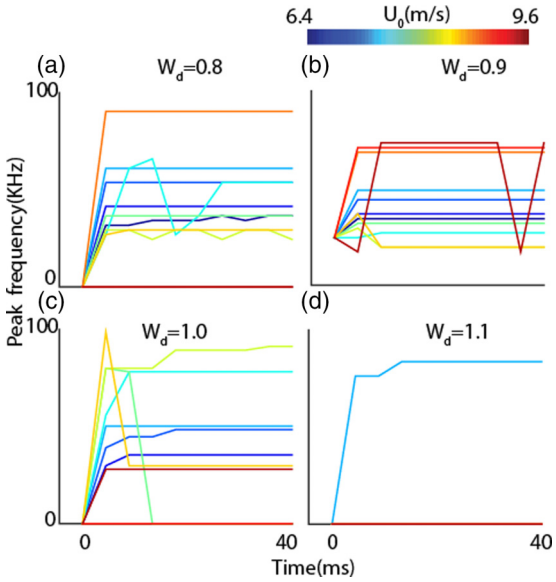

FIG. 5. Relation between f_p and U_{in} with variation in wedge distance (w_d). U_0 is varied from 6.4 ms^{-1} to 9.6 m/s in steps of 0.3 m/s, color-coded as shown by the color bar at the top. (a) w_d 0.8 mm, (b) w_d 0.9 mm, (c) w_d 1 mm, (d) w_d 1.1 mm.

overlap between adjoining segments. Most window functions taper off at the edges to avoid spectral ringing. The DFT of each windowed segment is added to a complex-valued matrix that contains the magnitude and phase for each point in time and frequency.

DFT is calculated using the following formula for a signal of length N:

$$X_m = \sum_{0}^{N-1} x(n)g(n - mR)e^{-j2\pi fn}. \tag{5}$$

There are variations in the spectrograms similar to mouse USVs. A few examples of the spectrograms generated are shown in Fig. 4. The examples shown in Fig. 4 are the following: three components with a nonharmonic relationship, low-frequency harmonics (observed mainly in females or during pain), syllables transiting from one pattern to another, syllables accompanied by a noiselike structure in between, single-frequency contours with and without a sudden jump in fundamental frequency, and harmonic and nonharmonic syllables (nonlinear components) [2,22].

B. Temporal analysis of the impact of different parameters

We wish to grab an understanding of the relationship of U_0 with f_p. Initially, the S_p is fixed at 1 mm, U_0 is varied in steps of 0.3 m/s in the range [6.4, 9.6 m/s], and wedge distance (w_d) is varied in steps of 0.1 mm within the limit of [0.8, 1.1]. The change in f_p over time is quantified using pitch contour as shown in Fig 5. Since the mouse USVs spectrogram may have sudden changes in frequency, instead of plotting mean peak frequency, we opt for pitch contours to get an insight into the modulation it undergoes over time in f_p. Interestingly, with the increase in inlet velocity, as shown in Fig. 5, there is a gradual increase in fundamental frequency that is consistent with the trends reported in the literature [16,25]. However, there are few outliers for which f_p decreases, and on further increase, no significant power spectral density is found. The above results are similar to those observed by Nyborg in 1952 [25] for jet edge systems, where he pointed out that few combinations would result in no significant output. For instance, in Fig. 5, for $w_d = 0.8$ (left top), the inlet velocity varies from 6.4 to 9.6 m/s in steps of 0.3 m/s, and the color map depicts the resultant change in pitch over time. For $U_0 = 6.4$ m/s, the pitch contour fluctuates over time between 25 and 29 kHz, with the mean being at 27 kHz. From 6.4 to 7.3 m/s, we see a gradual increase in f_p. At 7.7 m/s, the pitch again exhibits a fluctuation between 21 and 53 kHz, the mean being at 38 kHz. Surprisingly, as we go higher in U_0, from 8 to 8.6 m/s, the fundamental decreases to 29, 23, and 22 kHz, respectively. At $U_0 = 9$ m/s, it shoots up to about 72 kHz. On further increase in velocity, no pitch is detected as no significant power spectral density is observed. In Fig. 5, the color plots which are not visible are all 0, meaning the spectrograms lacked significant power spectral density above the threshold (mean + 2* standard deviation in our case). For $w_d = 0.9$ and 1, a similar trend is observed as for $w_d = 0.8$. However, for $w_d = 1.1$, only one combination leads to the generation of spectrograms with significant power spectral density. Thus, f_p works best for USVs with constant single frequency contour. Since USVs can also consist of sudden pitch jumps, upsweeps, and down sweeps for signals with single frequency components, pitch contour can thereby take us a step further in understanding the temporal variation in such signals. Pitch contours are therefore also computed for low, mid, and high values for each of the cases: inlet velocity parameter U_0 [7, 8, 9 (m/s)] (rounded values) with change in S_p [0.75, 1, 1.1 (mm)], W_{shift} [−0.0475, 0, +0.0475 (mm)] and diameter of the jet exit [0.17, 0.19, 0.21 (mm)] [low (blue), mid (green), and high (red)], as shown in Fig. 6. For all the cases under consideration, interestingly, for S_p at 1.1 mm, the f_p is less than others. For S_p at 1 mm, the f_p either remains comparable or increases with velocity, whereas for S_p at 0.75 mm, it exhibits a reverse trend. Positive W_{shift} fails to generate spectrograms with significant power spectral density at low and mid U_0. The mid values of the parameters, namely S_p, W_{shift}, and D_j, exhibit a similar trend over velocity with a substantial increase in f_p with velocities. Thus, sudden changes in f_p can be well seen in midchosen $U_0 = 7.7$ m/s for midvalued parameters (in green). There is a range beyond which no vocalizations can be generated for a particular set of combinations. Spectrograms of the same simulations with pitch contours as in Fig. 6 are shown in Fig. 7 for S_p and W_{shift}.

C. Removal of ventral pouch

While a group of researchers [16,21] presented solid evidential support for a jet-edge system and the criticality of the role of the VP in USV production, another group [18] claims that the sound is generated by a jet impingement setup, where the VP has no role to play. The latter group, however, focused mainly on generating the f_p (minimum, maximum, and average of f_p) components and not the spectrograms. Two vocalizations can have the same f_p but different distributions over time, contrasting each other. Nevertheless, the contradictory results shown by the above two groups create

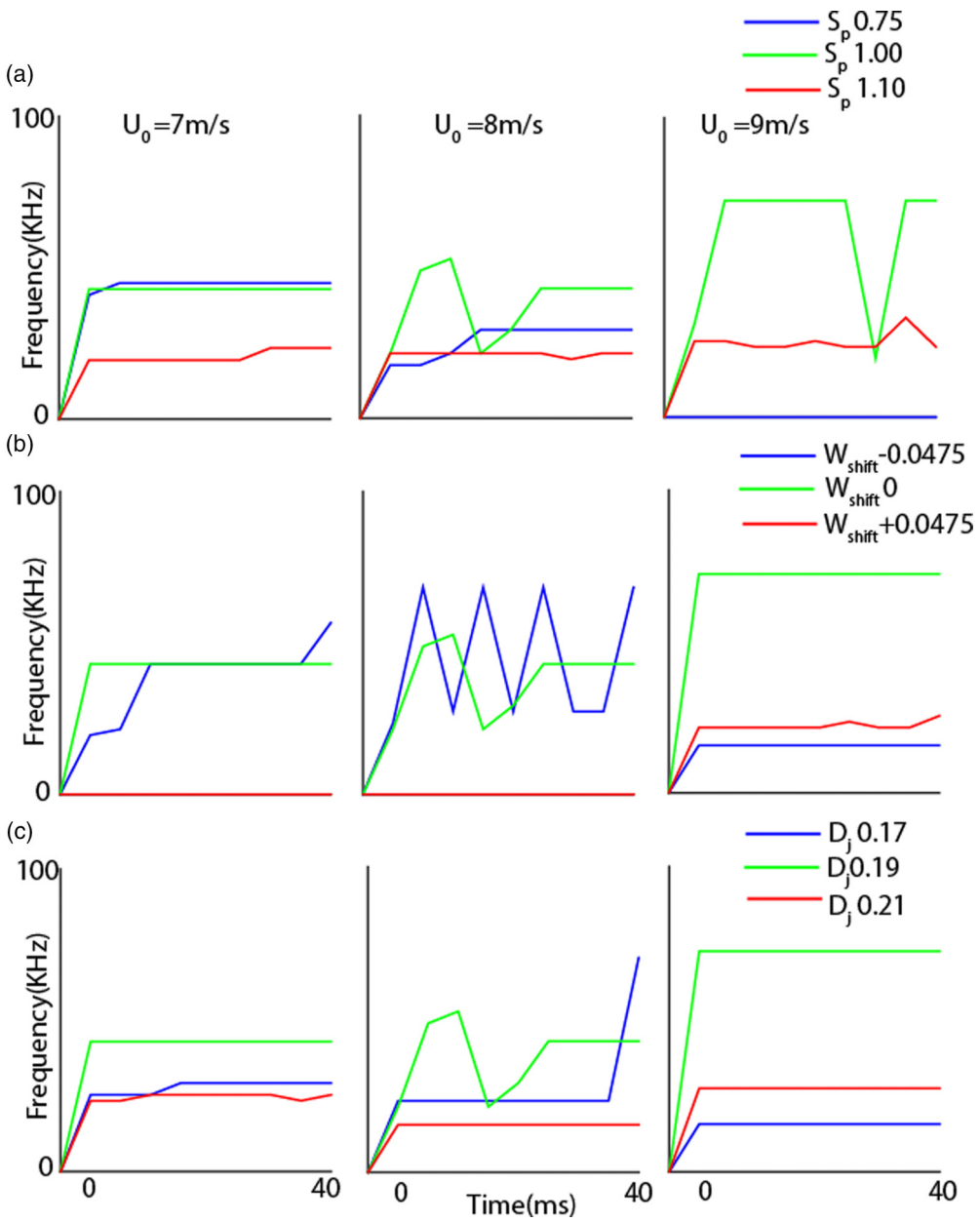

FIG. 6. Relation between f_0 and U_0 with variation in S_p (top), W_{shift} (middle), and diameter of jet exit (bottom) for three values low, mid, and high (rounded). (a) U_0 7 m/s, w_d 0.8 mm; (b) U_0 8 m/s, w_d 0.8 mm; (c) U_0 9 m/s, w_d 0.8 mm.

some intrigue regarding the exact role of the VP in USV production.

A cavity such as the VP is necessary and bound to be created for the edge placement to be viable, given the limited space in the larynx. Therefore, the blocking of the VP results in the removal of the alar edge. To understand this, the VP is removed in the previous model (Fig. 1), and the resulting setup, shown in Fig. 8, is used for simulations. Since blocking with metallic balls can give rise to new surfaces in the model [18], to avoid inducing such artificial artifacts, we opt for removal of the VP.

On removing the VP, the qualitative differences between the spectrograms are lost, and they transform into broadband distributions with a slight change in the frequency components, as shown in Fig. 9. The variation in pitch contour is shown to the right of the respective spectrograms with (blue) and without VP (red). For the mid U_0 (middle), no VP (W/O) and VP would have a similar f_p range which is similar to the observation reported by Håkansson in 2022 [18]. However, we can see that the fine structure in the spectrogram in the W/O case is missing. Surprisingly, with an increase in U_{in} for the VP cases, there is a gradual increase in f_p, but it remains the same for no VP. Pressure contours are further shown in Fig. 10, over three different time points (0.0125, 0.025, 0.0375 s). Interestingly, the flow seems to be parallel and there is no sign of impingement of the jet on the intralaryngeal wall as suggested by Mahrt 2016 [17] and Håkansson 2022 [18]. Rather, the source of disturbance in the laminar flow seems to be the alar edge with a significant amount of flow in VP. This leads to the generation of whistles thereby strengthening the

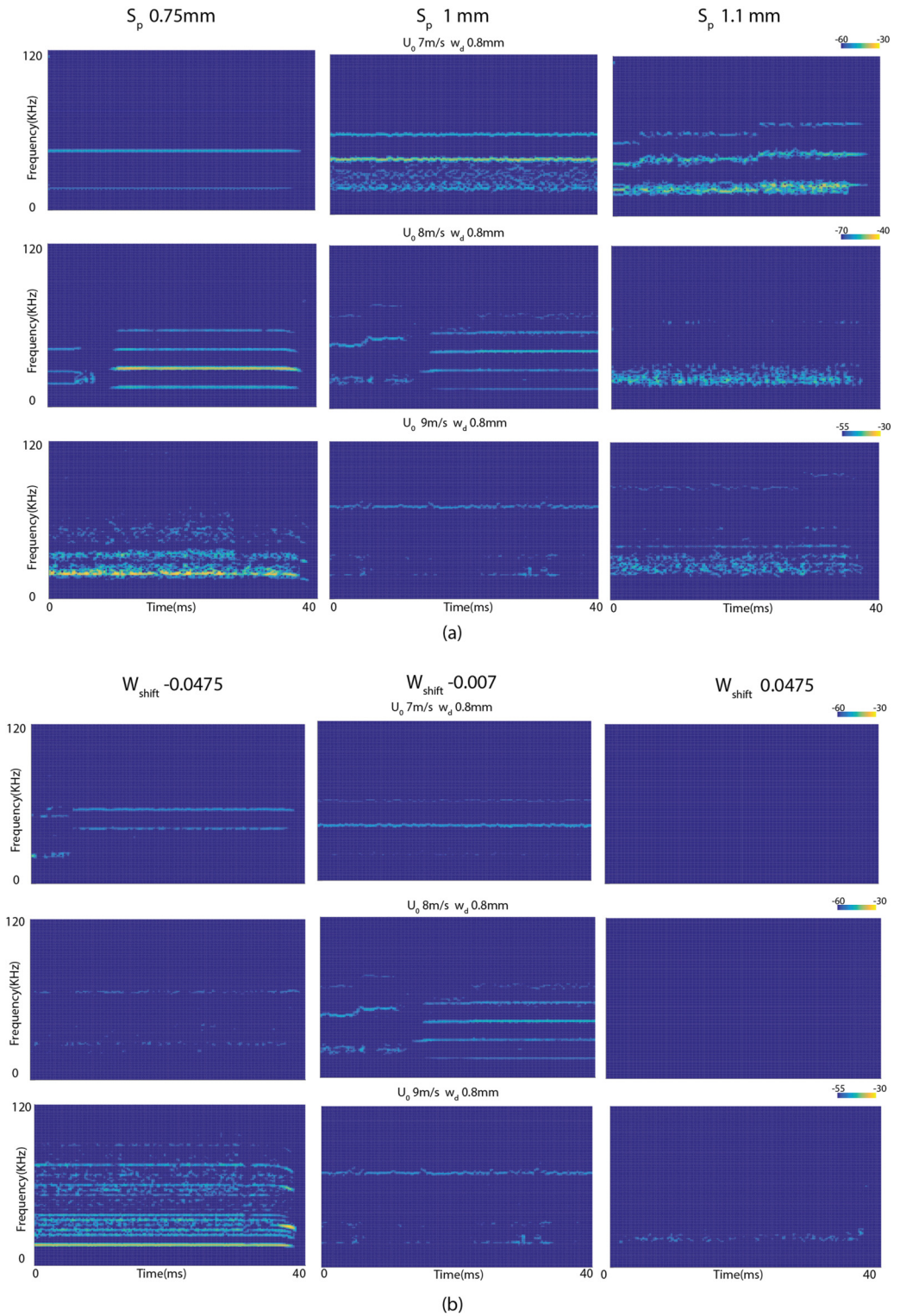

FIG. 7. Example spectrograms depicting effects of variation in (a) S_p, (b) W_{shift} parameters on the output vocalizations for U_0 7 m/s, w_d 0.8 mm (top row), U_0 8 m/s, w_d 0.8 mm (middle row), U_0 9 m/s, w_d 0.8 mm (third row).

role of the edge and pouch in generating different varieties of USVs modulated with change in U_{in}. The movies for two of the examples shown for the with and without VP [Figs. 9(b) and 9(c)] cases are added in the Supplemental Material [26].

As observed, for our computational model, the removal of the VP has a significant impact on characteristics of the spectrograms generated. In the aforementioned study supporting the jet impingement mechanism, the geometry had a curved surface immediately after the glottal constriction induced by the addition of an aluminium ball, making it conducive for the jet to impinge on the opposite wall and generate a whistle. Moreover, the sole focus of that study being on f_p of the

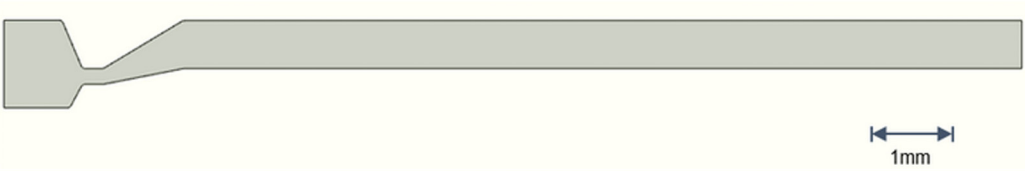

FIG. 8. Geometry with no ventral pouch.

vocalizations raises uncertainty about the inalterability of the USVs at the spectrographic level with the removal of VP. As in our study, the alar edge is the primary source of instability that is required for whistle generation, and its removal has a significant impact. Our results support the hypothesis that the VP in mice's larynx plays a crucial role in USV production and increases the variety of vocalizations that can be generated that are close to actual mice USVs.

One of our attempted geometries to model jet impingement is shown in Fig. 11. We have tried geometries similar to the geometry shown in [18] but in our case in the regime of parameters tested for all our simulations we did not obtain any acoustic structure in the spectrograms akin to mouse USVs.

III. CONCLUSION

Our study simulates a 2D laryngeal airway model close to the mouse anatomical structure. The model is capable of generating various pressure signals, whose spectrograms are similar to mouse USVs. This encouraged us to further vary the simulation model parameters within the permissible range, which generated variations in the spectrograms. We hypothesize that the laryngeal system is highly nonlinear and hence it has not been possible to observe any correlational relationship between the U_{in}, w_d, W_{shift}, S_p, and D_j parameters and the features of the output pressure signal. The changes in parameters do not result in deterministic changes in output spectrogram

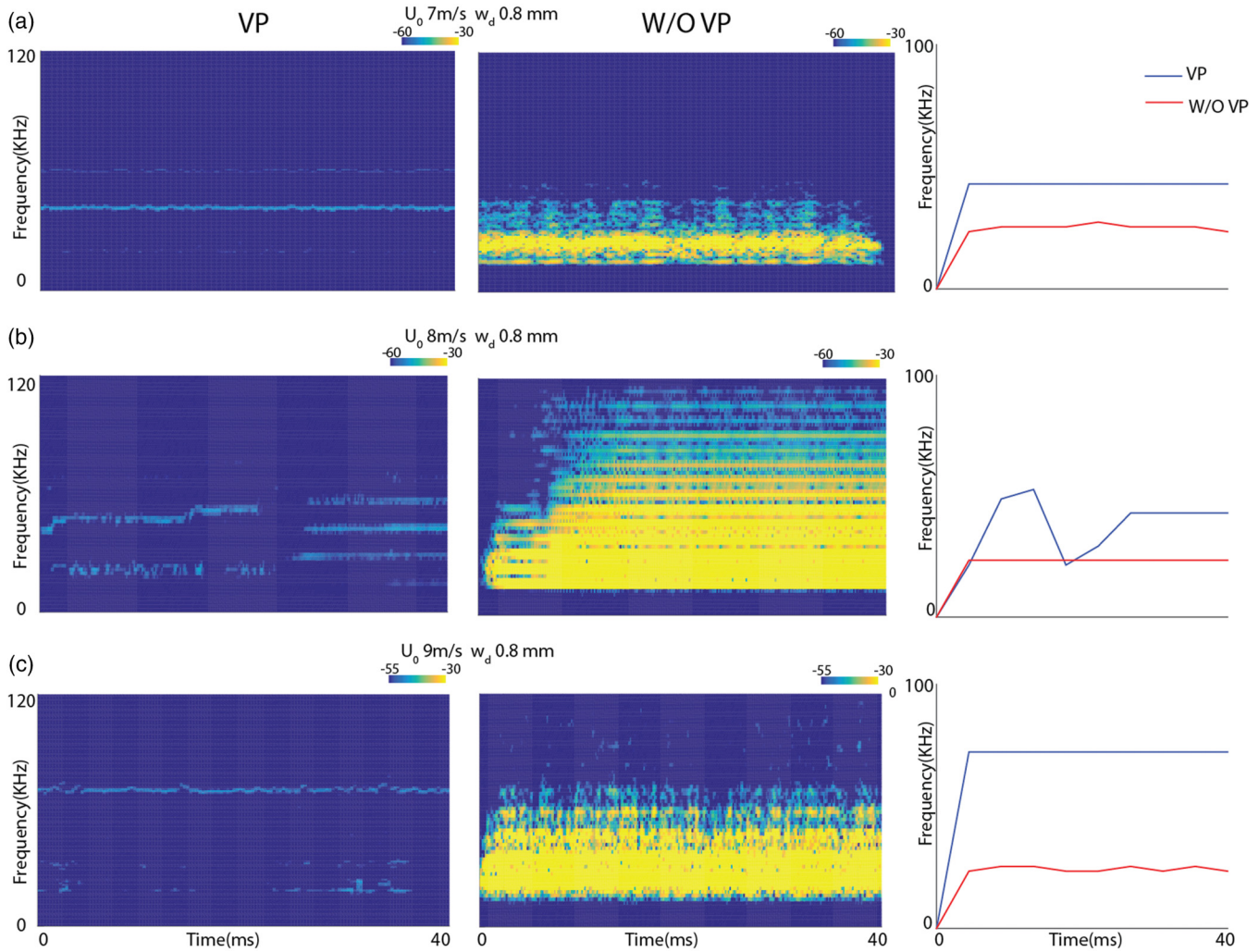

FIG. 9. Before (VP) (left) and after (W/O VP) (middle) removal of VP (a) U_0 7 m/s w_d 0.8 mm, (b) U_0 8 m/s w_d 0.8 mm, (c) U_0 9 m/s w_d 0.8 mm. Rightmost plot shows the pitch contour for VP (blue) and W/O VP (red) for each of the cases.

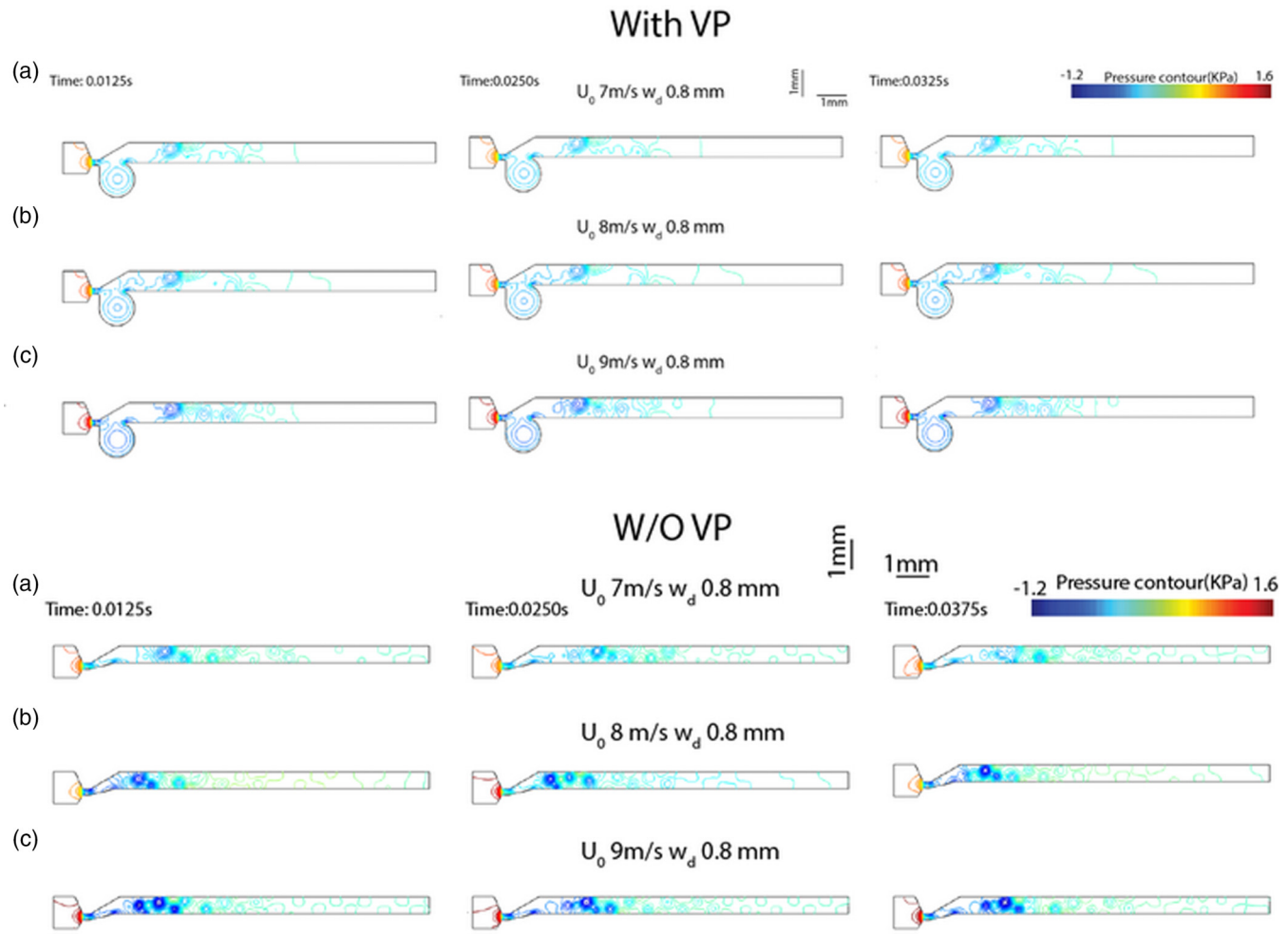

FIG. 10. Pressure contours with (VP) and after the removal of the ventral pouch (W/O VP). (a) U_0 7 m/s w_d 0.8 mm, (b) U_0 8 m/s w_d 0.8 mm, (c) U_0 9 m/s w_d 0.8 mm for three different time instants 0.0125 s (left), 0.0250 s (middle), and 0.375 s (right).

features, thus making it difficult to predict the impacts of different modifications. Significant qualitative changes in the spectrogram are observed with and without VP, validating the criticality of the structure as suggested previously. In summary, since VP and alar edge are crucial, our study provides evidence in support for jet edge rather than jet impingement as the identified aerodynamic mechanism driving the mouse USV production.

However, since our geometry is more complex, use of empirically determined loss coefficients (derived

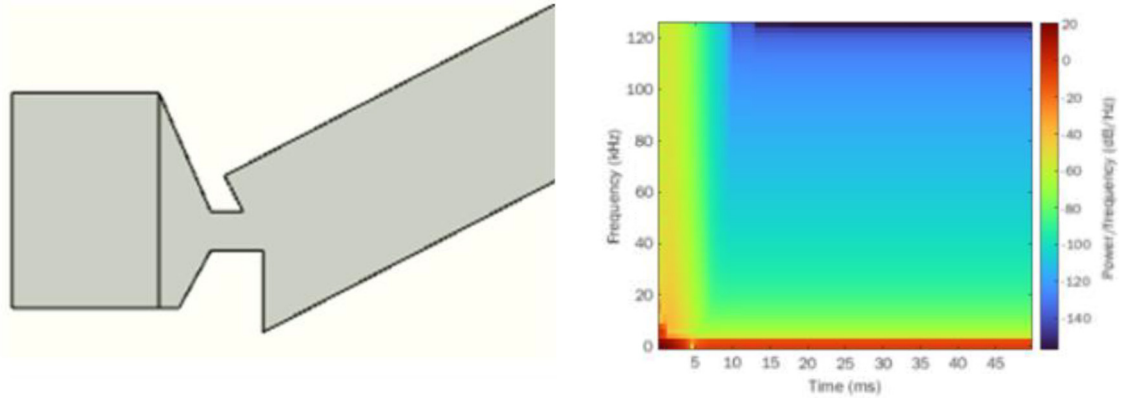

FIG. 11. Jet impingement simulation. Geometry used for the jet impingement simulation (left) with $U_0 = 8.5$ m/s. Spectrogram of the resultant output of the model is shown on the right.

for simpler geometries) would lead to inaccuracies. A finite element based computational fluid dynamic model solving the Navier-Stokes equation to obtain resultant parameters would result in more accurate results.

On another note, we have actually used a simplified idealized geometry. The current work can be extended by adding more realistic geometries in an incremental fashion to understand the specific role of different elements. Further, the basic structure we used, in reality, will be modified dynamically with motor inputs, so a number of steps and directions can be taken in asking questions based on the basic idealized structure.

ACKNOWLEDGMENTS

A.M. and S.A. thank MHRD for a Master's stipend and Institute Fellowship, respectively, and S.B. thanks IIT KGP for Challenge Grant funds. This work was supported by India-Czech Bilateral Scientific and Technological Cooperation DST India DST/INT/CZ/P-04/2020 and DST SERB Grant No. SERB-CRG/2021/005653 to S.B.

[1] T. E. Holy and Z. Guo, Ultrasonic songs of male mice, PLoS Biol. **3**, 12 (2005).

[2] J. Grimsley, S. Sheth, N. Vallabh, C. A. Grimsley, J. Bhattal, M. Latsko, and J. J. Wenstrup, Contextual modulation of vocal behavior in mouse: Newly identified 12 KHz "mid-frequency" vocalization emitted during restraint, Front. Behav. Neurosci. **10**, 38 (2016).

[3] E. Noirot and P. David, Sound analysis of ultrasonic distress calls of mouse pups as a function of their age, Anim. Behav. **17**, 340 (1969).

[4] G. Ehret and B. Haack, Motivation and arousal influence sound-induced maternal pup-retrieving behavior in lactating house mice, Z. Tierpsychol. **65**, 25 (1984).

[5] G. D. Sales, Ultrasound and aggressive behavior in rats and other small mammals, Anim. Behav. **20**, 88 (1972).

[6] D. T. Sangiamo, M. R. Warren, and J. P. Neunuebel, Ultrasonic signals associated with different types of social behavior of mice, Nat. Neurosci. **23**, 411 (2020).

[7] G. Ehret and B. Haack, Categorical perception of mouse pup ultrasound by lactating females, Naturwissenschaften **68**, 4 (1981).

[8] C. V. Portfors and D. J. Perkel, The role of ultrasonic vocalizations in mouse communication, Curr. Opinion Neurobiol. **28**, 115 (2014).

[9] J. Fischer and K. Hammerschmidt, Ultrasonic vocalizations in mouse models for speech and socio-cognitive disorders: Insights into the evolution of vocal communication, Genes, Brain and Behavior **10**, 17 (2011).

[10] S. Agarwalla, N. S. Arroyo, N. E. Long, W. T. O'Brien, T. Abel, and S. Bandyopadhyay, Male-specific alterations in structure of isolation call sequences of mouse pups with 16p11. 2 deletion, Genes, Brain Behavior **19**, 7 (2020).

[11] N. H. Fletcher, Air flow and sound generation in musical wind instruments, Ann. Rev. Fluid Mech. **11**, 123 (1979).

[12] J. Wolfe and J. Smith, Cutoff frequencies and cross fingerings in baroque, classical, and modern flutes, J. Acoust. Soc. Am. **114**, 4 (2003).

[13] C. M. Ho and S. Nosseir, Dynamics of an impinging jet. Part 1. The feedback phenomenon, J. Fluid Mech. **105**, 119 (1981).

[14] L. H. Roberts, The rodent ultrasound production mechanism, Ultrasonics **13**, 83 (1975).

[15] R. C. Chanaud, Aerodynamic whistles, Sci. Am. **222**, 1 (1970).

[16] T. Riede, H. L. Borgard, and B. Pasch, Laryngeal airway reconstruction indicates that rodent ultrasonic vocalizations are produced by an edge-tone mechanism, R. Soc. Open Sci. **4**, 11 (2017).

[17] E. Mahrt, A. Agarwal, D. Perkel, C. Portfors, and C. P. Elemans, Mice produce ultrasonic vocalizations by intra-laryngeal planar impinging jets, Curr. Biol. **26**, 19 (2016).

[18] J. Håkansson, W. Jiang, Q. Xue, X. Zheng, M. Ding, A. A. Agarwal, and C. P. Elemans, Aerodynamics and motor control of ultrasonic vocalizations for social communication in mice and rats, BMC Biol. **20**, 3 (2022).

[19] G. Smith, Structure of the normal rat larynx, Lab. Anim. **11**, 4 (1977).

[20] L. B. Thomas, J. C. Stemple, R. D. Andreatta, and F. H. Andrade, Establishing a new animal model for the study of laryngeal biology and disease: An anatomic study of the mouse larynx, Journal of Speech, Language, and Hearing Research **52**, 802 (2009).

[21] T. Riede and B. Pasch, Pygmy mouse songs reveal anatomical innovations underlying acoustic signal elaboration in rodents, J. Exp. Biol. **223**, jeb223925 (2020).

[22] C. V. Portfors, Types and functions of ultrasonic vocalizations in laboratory rats and mice, J. Am. Assoc. Lab. Anim. Sci. **46**, 28 (2007).

[23] J. M. Grimsley, J. J. Monaghan, and J. J. Wenstrup, Development of social vocalizations in mice, PLoS One **6**, 3 (2011).

[24] R. Ye, F. Cai, C. Guo, X. Zhang, Yan D, C. Chen, and B. Chen, Assessing the accuracy of ultrasound measurements of tracheal diameter: An in vitro experimental study, BMC Anesthes. **21**, 177 (2021).

[25] W. L. Nyborg, M. D. Burkhard, and H. K. Schilling, Acoustical characteristics of jet-edge and jet-edge-resonator systems, J. Acoust. Soc. Am. **24**, 3 (1952).

[26] See Supplemental Material at http://link.aps.org/supplemental/10.1103/PhysRevE.107.024412 for movies illustrating the air flow, with and without the ventral pouch, and jet impingement model simulation result.